

Lorentz Nonreciprocal Model for Hybrid Magnetoplasmonics

Dominik Floess,^{1,*} Thomas Weiss,¹ Sergei Tikhodeev,² and Harald Giessen¹

¹4th Physics Institute and Research Center SCOPE, University of Stuttgart, Stuttgart 70569, Germany

²A. M. Prokhorov General Physics Institute, Russian Academy of Sciences, Moscow 119991, Russia

(Received 21 March 2016; published 1 August 2016; corrected 5 August 2016)

Using localized surface plasmons, the magneto-optical response of dielectric thin films can be resonantly amplified and spectrally tailored. While the experimental realization and numerical simulation of such systems received considerable attention, so far, there is no analytical theoretical description. Here, we present a simple, intrinsically Lorentz nonreciprocal coupled oscillator model that reveals the underlying physics inside such systems and yields analytical expressions for the resonantly enhanced magneto-optical response. The predictions of the model are in good agreement with rigorous numerical solutions of Maxwell's equations for typical sample geometries. Our ansatz is transferable to other complex and hybrid nano-optical systems and will significantly facilitate device design.

DOI: 10.1103/PhysRevLett.117.063901

Hybrid magneto-optical (MO) and plasmonic materials have recently attracted a lot of interest, as this combination allows for magnetic tuning as well as for nonreciprocal effects [1–8]. By leveraging localized plasmon modes, the MO response of conventional materials can be resonantly amplified and spectrally tailored.

In the simplest approach, metallic MO nanoparticles [9–13] are utilized to enhance the MO response in reflection geometry (i.e., the MO Kerr effect). A significantly stronger MO response can be achieved in transmission [14–17]. Here, the polarization plane of the transmitted light is rotated by an angle that is proportional to the magnetic field and to the material thickness. This effect is termed Faraday effect [18].

It was shown recently that the Faraday rotation [14] and also the transverse MO Kerr effect [4] of a dielectric MO film can be enhanced by an order of magnitude through inclusion of a resonant plasmonic grating leading to a waveguide-plasmon-polariton (WPP) dispersion [19,20]. By varying the grating and nanowire geometry, the maximal polarization rotation enhancement can be tuned to arbitrary spectral positions [15]. Such structures exhibited a Faraday rotation of up to 4.2° for a thickness of 220 nm, while maintaining a high transmission of over 25% [15]. Hence, they are very relevant for possible devices, such as thin-film Faraday rotators and isolators as their performance data exceed other approaches considerably.

In this Letter, we present a simple coupled oscillator model that unravels the relation between the WPP quasi-particle and the enhanced Faraday rotation of such systems by providing analytical expressions for the magneto-optical response. The Lorentz nonreciprocity of the oscillator model is intrinsically incorporated via the Lorentz force, which is proportional to $\mathbf{v} \times \mathbf{B}$.

The geometry of such a hybrid structure is depicted in Fig. 1(a). It consists of a dielectric MO thin film with an

attached one-dimensional gold grating on top. The incident light is assumed to be linearly polarized and impinges on the sample along the z direction. The polarization direction with an electric field perpendicular (parallel) to the gold wires will be referred to as $x(y)$ polarized. Figure 1(b) depicts the corresponding mechanical analog of the optical system, where each relevant optical excitation is represented by a mass suspended by a linear spring. The coupling between the different excitations is modeled by interconnecting springs. All masses are assumed to be charged and driven by the external light field. Because of its periodicity, the gold grating acts primarily as a waveguide coupler and allows for the far-field excitation of transverse electric (TE) and transverse magnetic (TM) polarized quasiguided waveguide modes inside the MO film. In the absence of the magnetic field, the TE (TM) waveguide modes can only be excited by $y(x)$ polarized incident light. Thus, the waveguide modes are modeled by one mass each, which is restricted to move only along the x or y

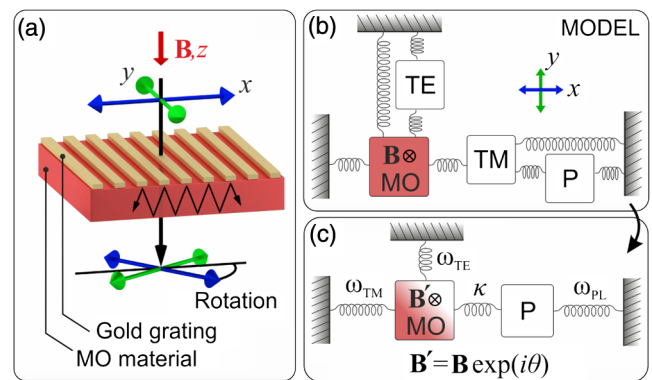


FIG. 1. (a) Schematic drawing of the hybrid magnetoplasmonic nanostructure. (b) Mechanical analog that represents the coupling of the relevant optical excitations. (c) Simplified oscillator model providing analytical solutions.

direction. The second purpose of the gold wires is to provide a localized plasmon resonance, which can be excited for x -polarized light. This plasmonic resonance is taken into account by an oscillator moving in x direction (labeled P). Because of the field overlap, the plasmonic resonance is coupled to the TM waveguide mode [19,20]. The dielectric response of the MO material itself is modeled by the red mass, which can move within the xy plane and is subjected to a Lorentz force [21] in the xy plane due to a static magnetic field \mathbf{B} oriented along the z direction.

The oscillator system in Fig. 1(b) possesses 5 degrees of freedom. Its motion is described by five coupled second order linear differential equations. While these equations can be solved exactly, it is impossible to derive closed expressions for its eigenmode frequencies. To simplify the model and allow for the analytical calculation of the eigenmode frequencies, a series of proper approximations can be applied.

First of all, neglecting the dispersion effects by the MO material itself yields significant simplification. This is achieved by assuming the driving frequency to be far away from the MO oscillator resonance and the impact of the driving force on the MO oscillator (i.e., the associated coupling constant) to be relatively small, resulting in a reduced system of three coupled second order equations. Furthermore, in a rotating wave approximation, which is valid when the driving frequency ω is close to the eigenfrequencies Ω_j ($j = \text{TE, TM, P}$) of the individual oscillators, the second order equations are reduced to first order. The mathematical details of the model reduction are provided in the Supplemental Material [22] and the limitations of the applied approximations are discussed later in this article.

The simplified oscillator scheme is depicted in Fig. 1(c). The three masses of the TE, TM, and material oscillator are now merged into one waveguide oscillator. Assuming a time-harmonic oscillator displacement that is proportional to $\exp(-i\omega t)$, the governing equations in the rotating wave approximation are given by the matrix equation

$$(M_0 + \Delta M - I\omega)\mathbf{x} = \eta R \mathbf{E}_{\parallel}, \quad (1)$$

where I is the 3×3 identity matrix, and η is a residue of the rotating wave approximation that is inversely proportional to the effective mass and the density of our oscillators [22]. The vector $\mathbf{x} = (x_{\text{TM}}, x_{\text{P}}, y_{\text{TE}})^T$ contains the displacements of the corresponding oscillators in the xy plane, while $\mathbf{E}_{\parallel} = (E_x, E_y)^T$ denotes the driving electric field. The forces acting on each oscillator are proportional to $R \mathbf{E}_{\parallel}$, with the charge density matrix

$$R = \begin{pmatrix} \rho_{\text{TM}} & 0 \\ \rho_{\text{P}} & 0 \\ 0 & \rho_{\text{TE}} \end{pmatrix}. \quad (2)$$

Furthermore, M_0 accounts for the coupling of the TM waveguide mode and plasmon [19], with

$$M_0 = \begin{pmatrix} \omega_{\text{TM}} & -\kappa & 0 \\ -\kappa & \omega_{\text{P}} & 0 \\ 0 & 0 & \omega_{\text{TE}} \end{pmatrix}. \quad (3)$$

The corresponding coupling constant κ is assumed to be purely real, while $\omega_j = \Omega_j - i\Gamma_j$, ($j = \text{TE, TM, P}$) are complex frequencies that consist of the resonance frequencies Ω_j and the damping coefficients Γ_j (due to radiative and absorptive losses) of the different modes. The anti-symmetric matrix ΔM denotes the nonreciprocal influence of the magnetic field via the Lorentz force proportional to $\mathbf{v} \times \mathbf{B}$ and is defined as

$$\Delta M = \beta e^{i\theta} \begin{pmatrix} 0 & 0 & -i \\ 0 & 0 & 0 \\ +i & 0 & 0 \end{pmatrix}, \quad (4)$$

with the real coupling coefficient β that is proportional to the static magnetic field. The factor $\exp i\theta$ stems from the four-oscillator model and represents the phase of the MO oscillator in that system. In Secs. III and VI of Ref. [22] it is shown by perturbation theory [23,24] that this phase corresponds to the phase of the gyration $g = |g| \exp(i\theta)$ of the MO material.

The optical response of the system is obtained by assigning an effective susceptibility to the system. This is done by summing up the effective electronic polarization $\mathbf{P}_{\parallel} = \chi \mathbf{E}_{\parallel}$, which can be identified as $\mathbf{P}_{\parallel} = R^T \mathbf{x}$. Hence, the effective susceptibility can be written as

$$\chi(\omega) = \eta R^T M(\omega)^{-1} R, \quad (5)$$

with $M(\omega) = M_0 + \Delta M - I\omega$. Because of the cross product in the Lorentz force, ΔM and thus $M(\omega)$ become antisymmetric for nonzero magnetic fields, reflecting the nonreciprocity of the system [25,26].

The eigenfrequencies of the coupled oscillator system are obtained by setting the external electric field in Eq. (1) to zero. This results in the following eigenvalue problem:

$$(M_0 + \Delta M)\mathbf{x}_n = \omega_n \mathbf{x}_n, \quad (6)$$

where ω_n denotes the eigenvalues, and \mathbf{x}_n the eigenvectors for $n = 1, 2, 3$. In our model, the Lorentz force is assumed to be weak compared to the restoring forces. Hence, ΔM is regarded as a small perturbation of M_0 , resulting in ω_n being close to the eigenfrequencies of M_0 . The eigenfrequencies of M_0 are given by

$$\omega_{1/2} = \frac{\omega_{\text{TM}} + \omega_{\text{P}}}{2} \mp \sqrt{\kappa^2 + \left(\frac{\omega_{\text{TM}} - \omega_{\text{P}}}{2}\right)^2}, \quad (7)$$

$$\omega_3 = \omega_{\text{TE}}. \quad (8)$$

The first two eigenfrequencies correspond to the two branches of a WPP hybrid mode arising from the coupling between the plasmonic mode and the TM waveguide mode [19,20]. The third eigenfrequency is simply the frequency of the TE polarized waveguide mode. In earlier work, it was demonstrated numerically [14,15] that the largest magneto-optical response occurs for grating periods at which the TE waveguide mode and one of the TM polarized WPP branches possess similar resonance frequencies, i.e., when $\omega_{1/2} = \omega_{\text{TE}}$. This behavior can now be deduced *analytically* from the presented model by examining the inverse of M for a small perturbation ΔM :

$$M^{-1} \approx (M_0 - I\omega)^{-1} - \frac{i\beta e^{i\theta}}{(\omega_1 - \omega)(\omega_2 - \omega)(\omega_{\text{TE}} - \omega)} \times \begin{pmatrix} 0 & 0 & +(\omega - \omega_p) \\ 0 & 0 & -\kappa \\ -(\omega - \omega_p) & +\kappa & 0 \end{pmatrix}. \quad (9)$$

This expression reveals that the magnetic terms proportional to β become largest for $\omega = \omega_{\text{TE}} = \omega_{1/2}$, which confirms previous numerical findings.

To obtain the effective susceptibility for a particular nanostructure, the free parameters in M and R have to be deduced by a systematic and rigorous fitting procedure. Our fitting process consists of three steps, in which M_0 , R , and ΔM are fitted sequentially. Full numerical simulations based on the scattering matrix method [27,28] were used as reference. In the following, the three fitting steps are discussed and applied to a sample geometry that consists of a 150 nm thick EuSe film with 70 nm thick and 70 nm wide gold wires on top [see Fig. 1(a)]. The substrate under the film is assumed to be glass. The applied magnetic field was assumed to be 5 T. For the dielectric function of gold, we used a Drude model with parameters given by Ref. [1], whereas the other dielectric components were assumed to have a constant dielectric function (see Sec. IV in Ref. [22]).

In the first step, the free parameters in M_0 are fitted such that the eigenfrequencies of the mechanical system match the eigenfrequencies of the actual nanostructure obtained by rigorous numerical solutions of Maxwell's equations. While Eq. (8) allows the direct derivation of ω_{TE} , the complex coefficients ω_{TM} , ω_p , and the real coefficient κ in Eq. (7) cannot be deduced directly from the full numerical simulations. This can be resolved by calculating the real part of ω_{TM} from an empty lattice approximation [29] and assuming $\Gamma_{\text{TM}} \approx \Gamma_{\text{TE}}/10$, as justified by the results in Refs. [19,20]. Figure 2 shows the comparison between the simulated and fitted eigenmodes of the oscillator model that includes the Lorentz force. The eigenmodes are plotted as blue (TM) and green (TE) dashed lines in units of wavelength. The solid black lines mark the edge of the light cone (i.e., the Rayleigh anomaly). The blue solid lines correspond to the frequencies of the individual oscillators.

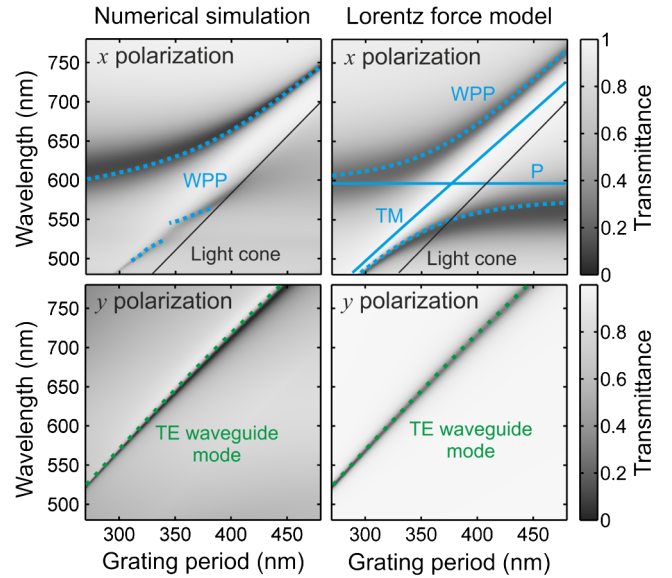


FIG. 2. Comparison between transmittance spectra and modal dispersion derived from numerical simulations (left panels) and the Lorentz force oscillator model (right panels). TM (TE) polarized modes are plotted as blue (green) dashed lines. Blue solid lines indicate the uncoupled plasmon and TM waveguide frequencies.

Especially in the most relevant region around the intersection of the TE waveguide mode and WPP, the modal dispersion is reproduced very well by the oscillator model. Outside this region, in the simulated TM dispersion at around 530 nm, there is a discontinuity due to the presence of another spectrally close higher-order mode. As expected [30], the eigenmodes of the actual nanostructure exhibit a cutoff at the edge of the light cone. Since the model does not take the periodic geometry into account, this discontinuity is missing in the dispersion plot of the model.

In the second part of the fitting sequence, the coefficients in R are derived by the condition that the transmittance of the effective medium has to reproduce that of the actual sample. In analogy to the first fitting step, it is assumed that the magnetic field exhibits only a weak influence on the absorption behavior. Hence, the absorption can be derived from the effective susceptibility for zero B field. This is done by setting $\Delta M = 0$ and solving the Helmholtz equation to obtain the evolution of an x - and y -polarized plane wave over an effective propagation distance. This distance was assumed to be the sample thickness of 220 nm. For the sake of simplicity, the coefficients in R were assumed to be constant for all grating periods. By comparing the simulated transmittance in Fig. 2 (left panels) and the modeled transmittance (right panels), it can be seen that, except for the discontinuities outside the region of interest, as discussed above, the line shapes agree very well.

In the third part of the fitting procedure, the remaining magneto-optical coefficients in ΔM are determined. Far away from the MO material resonance, the gyration

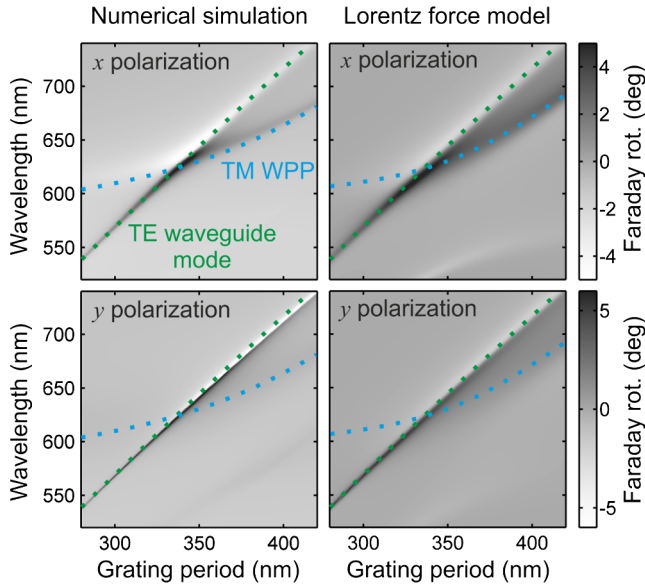


FIG. 3. Comparison of the Faraday rotation derived from numerical simulations (left panels) and the Lorentz force oscillator model (right panels). The eigenfrequencies corresponding to the upper TM polarized waveguide plasmon polariton (WPP) branch and the TE waveguide mode are drawn as dashed lines.

$g = |g| \exp(i\theta)$ can be assumed to be constant. For bismuth iron garnet [14] and EuSe [15], this assumption is valid for the red and near-IR spectral region, where $\theta \approx -45^\circ$. This is also the value used for the oscillator model and the numerical simulations. Note that our model will work as well for other materials exhibiting different θ (see Sec. VI in Ref. [22]). The last remaining fitting parameter is β , which is proportional to the magnetic field. For realistic magnetic field strengths, its value only influences the magnitude of the MO response but not its spectral line shape. Therefore, we scale β such that the MO response of the modeled system reaches the values of the full simulation.

Figure 3 depicts the comparison of the resulting Faraday rotation spectra from the full numerical simulations and our oscillator model. The green and blue dotted lines trace the eigenmodes. As expected by examining Eq. (9), the MO response is largest around the intersection point of the TM polarized WPP and the TE waveguide mode. Furthermore, the qualitative and quantitative agreement between model and numerical simulation is excellent. The corresponding dispersion of ellipticity can be found in Sec. V in Ref. [22]. To compare the exact line shapes of the MO spectra, Fig. 4 displays the corresponding slice cuts of the Faraday rotation and ellipticity spectra. Our model reproduces the line shapes very well [31]. This includes the characteristic up-down feature in the Faraday rotation for x polarization (indicated by arrows), which successively exhibits larger spectral separation for periods larger than that of the TE-WPP intersection (green line). This was also observed in Ref. [15]. The only difference is that the modeled MO spectra do not reproduce the offset in the spectra from the

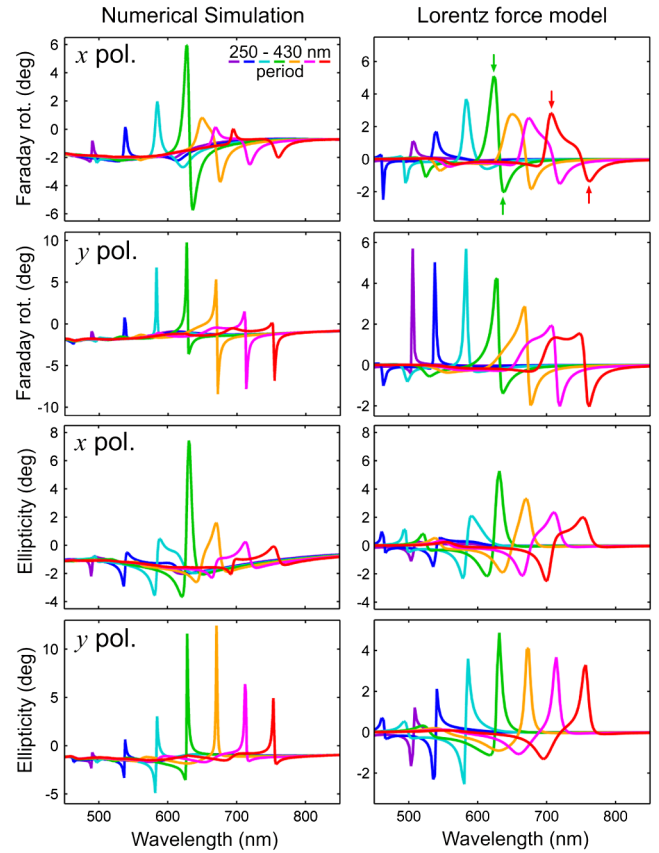


FIG. 4. Comparison of Faraday rotation and ellipticity derived from numerical simulations (left panels) and the Lorentz force oscillator model (right panels). The spectra correspond to slice cuts from Fig. 3 at equidistant periods from 250 nm to 430 nm with 30 nm spacing.

numerical simulation. This is a result of the approximations required for the reduction of the four-oscillator model to the two-oscillator model. There, the oscillator strength of the MO material was assumed to be much smaller than the oscillator strength of the waveguide modes and the plasmon. As a result, only the resonant contributions to the MO response are taken into account.

In summary, the dispersion of the MO response of hybrid magnetoplasmonic waveguides can now be understood in the picture of a simple oscillator model including the nonreciprocal Lorentz force. In the case of weak influence of the Lorentz force, analytical expressions for the optical response were obtained, which confirm previous numerical findings. Importantly, the spectral line shape of the MO response is fully determined by the optical properties of the system for zero magnetic field. Only the overall magnitude of the MO response is determined by the applied magnetic field.

The theory in this article provides the understanding required to further develop hybrid magnetoplasmonic systems in highly integrated optics, demanding actively controlled optical modulation [32], magnetic field sensing [33,34], refractive index sensing [35], and optical isolation

[36–41]. It should also be mentioned that the presented findings can not only help to understand and optimize existing sample geometries, but can also be transferred to other geometries, such as 2D plasmonic gratings. Furthermore, by removing all plasmonic oscillators, the case of a purely dielectric grating-waveguide combination can be realized.

In prospect of nonlinear magnetoplasmonics, the presented model could also be of fundamental relevance. Although the described model is fully linear, a nonlinear extension would be straightforward by adding higher order coupling terms [42].

The authors acknowledge support from DFG (SPP 1839, Mercator-Professorship), BMBF (13N12443 Faraday), MWK Baden-Württemberg (Zukunftsoffensive IV), ERC Complexplas, and RFBR (14-02-00778 and 16-29-03282).

*Corresponding author.

d.floess@pi4.uni-stuttgart.de

- [1] V. I. Belotelov, L. L. Doskolovich, and A. K. Zvezdin, *Phys. Rev. Lett.* **98**, 077401 (2007).
- [2] V. V. Temnov, G. Armelles, U. Woggon, D. Guzatov, A. Cebollada, A. Garcia-martin, T. Thomay, A. Leitenstorfer, and R. Bratschitsch, *Nat. Photonics* **4**, 107 (2010).
- [3] V. Belotelov, I. Akimov, M. Pohl, V. Kotov, S. Kasture, A. Vengurlekar, A. Gopal, D. Yakovlev, A. Zvezdin, and M. Bayer, *Nat. Nanotechnol.* **6**, 370 (2011).
- [4] L. E. Kreilkamp, V. I. Belotelov, J. Y. Chin, S. Neutzner, D. Dregely, T. Wehlius, I. A. Akimov, M. Bayer, B. Stritzker, and H. Giessen, *Phys. Rev. X* **3**, 041019 (2013).
- [5] V. I. Belotelov, L. E. Kreilkamp, I. A. Akimov, A. N. Kalish, D. A. Bykov, S. Kasture, V. J. Yallapragada, A. Venu Gopal, A. M. Grishin, S. I. Khartsev, M. Nur-E-Alam, M. Vasiliev, L. L. Doskolovich, D. R. Yakovlev, K. Alameh, A. K. Zvezdin, and M. Bayer, *Nat. Commun.* **4**, 2128 (2013).
- [6] A. R. Davoyan and N. Engheta, *Phys. Rev. Lett.* **111**, 047401 (2013).
- [7] S. Fan, *Nat. Photonics* **4**, 76 (2010).
- [8] A. B. Khanikaev, S. H. Mousavi, G. Shvets, and Y. S. Kivshar, *Phys. Rev. Lett.* **105**, 126804 (2010).
- [9] P. K. Jain, Y. Xiao, R. Walsworth, and A. E. Cohen, *Nano Lett.* **9**, 1644 (2009).
- [10] B. Sepúlveda, J. B. González-Díaz, A. García-Martín, L. M. Lechuga, and G. Armelles, *Phys. Rev. Lett.* **104**, 147401 (2010).
- [11] J. B. González-Díaz, B. Sepúlveda, A. García-Martín, and G. Armelles, *Appl. Phys. Lett.* **97**, 043114 (2010).
- [12] J. C. Banthí, D. Meneses-Rodríguez, F. García, M. U. González, A. García-Martín, A. Cebollada, and G. Armelles, *Adv. Mater.* **24**, OP36 (2012).
- [13] M. Kataja, T. K. Hakala, A. Julku, M. J. Huttunen, S. van Dijken, and P. Törmä, *Nat. Commun.* **6**, 7072 (2015).
- [14] J. Y. Chin, T. Steinle, T. Wehlius, D. Dregely, T. Weiss, V. I. Belotelov, B. Stritzker, and H. Giessen, *Nat. Commun.* **4**, 1599 (2013).
- [15] D. Floess, J. Y. Chin, A. Kawatani, D. Dregely, H.-U. Habermeier, T. Weiss, and H. Giessen, *Light Sci. Appl.* **4**, e284 (2015).
- [16] T. Körner, A. Heinrich, M. Weckerle, P. Roocks, and B. Stritzker, *J. Appl. Phys.* **103**, 07B337 (2008).
- [17] J. C. Suits and B. E. Argyle, *J. Appl. Phys.* **36**, 1251 (1965).
- [18] P. N. Schatz and A. J. McCaffery, *Q. Rev. Chem. Soc.* **23**, 552 (1969).
- [19] A. Christ, S. G. Tikhodeev, N. A. Gippius, J. Kuhl, and H. Giessen, *Phys. Rev. Lett.* **91**, 183901 (2003).
- [20] A. Christ, T. Zentgraf, J. Kuhl, S. G. Tikhodeev, N. A. Gippius, and H. Giessen, *Phys. Rev. B* **70**, 125113 (2004).
- [21] G. R. Fowles, *Introduction to Modern Optics*, 2nd ed. (Dover Publications, New York, 1975).
- [22] See Supplemental Material at <http://link.aps.org/supplemental/10.1103/PhysRevLett.117.063901> for details on the model simplification, simulation parameters, and perturbation theory.
- [23] M. B. Doost, W. Langbein, and E. A. Muljarov, *Phys. Rev. A* **90**, 013834 (2014).
- [24] T. Weiss, M. Mesch, M. Schäferling, H. Giessen, W. Langbein, and E. A. Muljarov, *Phys. Rev. Lett.* **116**, 237401 (2016).
- [25] S. Fan, R. Baets, A. Petrov, Z. Yu, J. D. Joannopoulos, W. Freude, A. Melloni, M. Popović, M. Vanwolleghem, D. Jalas, M. Eich, M. Krause, H. Renner, E. Brinkmeyer, and C. R. Doerr, *Science* **335**, 38 (2012).
- [26] A. T. de Hoop, *Appl. Sci. Res., Sect. B* **8**, 135 (1960).
- [27] T. Weiss, G. Granet, N. A. Gippius, S. G. Tikhodeev, and H. Giessen, *Opt. Express* **17**, 8051 (2009).
- [28] T. Weiss, N. A. Gippius, S. G. Tikhodeev, G. Granet, and H. Giessen, *J. Opt. Soc. Am. A* **28**, 238 (2011).
- [29] S. G. Tikhodeev, A. L. Yablonskii, E. A. Muljarov, N. A. Gippius, and T. Ishihara, *Phys. Rev. B* **66**, 045102 (2002).
- [30] A. B. Akimov, N. A. Gippius, and S. G. Tikhodeev, *JETP Lett.* **93**, 427 (2011).
- [31] The slightly broader MO features result from fitting the resonance linewidths to the values from numerical simulations. A better qualitative agreement in Faraday rotation could be obtained when adjusting the losses in our model independently of the calculated resonance linewidths.
- [32] W. E. Ross, D. Psaltis, and R. H. Anderson, *Opt. Eng.* **22**, 224485 (1983).
- [33] L. Sun, S. Jiang, and J. R. Marciante, *Opt. Express* **18**, 5407 (2010).
- [34] M. Deeter, A. Rose, and G. Day, *J. Lightwave Technol.* **8**, 1838 (1990).
- [35] N. Maccaferri, K. E. Gregorczyk, T. V. a. G. de Oliveira, M. Kataja, S. van Dijken, Z. Pirzadeh, A. Dmitriev, J. Åkerman, M. Knez, and P. Vavassori, *Nat. Commun.* **6**, 6150 (2015).
- [36] M. Shirasaki and K. Asama, *Appl. Opt.* **21**, 4296 (1982).
- [37] L. Bi, J. Hu, P. Jiang, and D. Kim, *Nat. Photonics* **5**, 758 (2011).
- [38] L. Fan, J. Wang, L. T. Varghese, H. Shen, B. Niu, Y. Xuan, A. M. Weiner, and M. Qi, *Science* **335**, 447 (2012).
- [39] I. Ikushima and M. Maeda, *IEEE J. Quantum Electron.* **14**, 331 (1978).
- [40] T. Morikawa, Y. Mitsuhashi, J. Shimada, and Y. Kojima, *Electron. Lett.* **12**, 435 (1976).
- [41] K. Petermann, *IEEE J. Sel. Top. Quantum Electron.* **1**, 480 (1995).
- [42] B. Metzger, M. Hentschel, M. Lippitz, and H. Giessen, *Opt. Lett.* **37**, 4741 (2012).